Available online at www.sciencedirect.com
ScienceDirect
International Journal of Heat and Mass Transfer 51 (2008) 2657–2664
International Journal of HEAT and MASS TRANSFER
www.elsevier.com/locate/ijhmt

Combined effects of thermophoresis and electrophoresis on particle deposition onto a wavy surface disk

Chieh-Li Chen [a,*], Kun-Chieh Chan [b]

[a] Department of Aeronautics and Astronautics, National Cheng Kung University, Tainan 70101, Taiwan
[b] Department of Mechanical Engineering, National Cheng Kung University, Tainan 70101, Taiwan

Received 19 December 2006; received in revised form 27 September 2007
Available online 3 December 2007

Abstract

In this paper, the coordinate transformation method is used to analyze the aerosol particle deposition from a stagnation flow onto an axisymmetric wavy disk under to the coupling effects of Brownian diffusion, convection, sedimentation, thermophoresis and electrophoresis. The transformed governing equations obtained by coordinate transformation are solved by the spline alternating-direction implicit method. Numerical results show that electrophoresis will increase the particle deposition effect. It reveals that the thermophoresis effect of the cold wall will induce a driving effort to force particles toward the wall and accelerate the deposition onto the wall. When Brownian diffusion and thermophoresis dominate the particle deposition process, the influence of the lumpy surface geometry will become stronger with the increase of the disk radius, and the mean particle deposition effect of the wavy disk would be less than that of the flat disk.

Keywords: Thermophoresis; Electrophoresis; Stagnation flow; Wavy surface; Cubic spline

1. Introduction

Recently, studies in aerosol deposition have become more and more important for engineering applications. In particular, the contaminant particle deposition onto the surface of products in the electronic industry plays a critical role in the resulting product quality. The factors that influence particle deposition include convection, Brownian diffusion, turbulence, sedimentation, inertial effect, thermophoresis, electrophoresis and surface geometry, respectively. Among these factors, thermophoresis is important for $0.1\ \mu m < d_p < 1\ \mu m$, convection, Brownian diffusion, and electrophoresis are important for $d_p < 0.1\ \mu m$, and inertial effect and sedimentation are important for $d_p > 1\ \mu m$. The velocity caused by thermophoresis is called thermophoretic velocity [1]. There were some studies [2,3] that considered the particle deposition onto a flat plate involving Brownian diffusion and thermophoresis. These studies show that a cold wall surface will lead to an increase of particle deposition due to thermophoresis. Ye et al. [4] studied the effect of thermophoresis on deposition rate experimentally and numerically. Cooper et al. [5] predicted deposition velocity in viscous axisymmetric stagnation flows by convection–diffusion velocity and electrophoretic velocity. The boundary layer approximation and the perturbation method are applied to solve the transport equation and determine the particle deposition by [6]. Opiolka et al. [7] used the stagnant film model to examine the deposition rates and conducted an experimental study. Tsai et al. [8] represented a similarity analysis to study the particle deposition and deposition velocity involving thermophoresis and electrophoresis from a two-dimensional axisymmetric air flow around a wafer. As to the study for system with complex boundary, there were many works in heat transfer for irregular boundary [9,10]. The combined effect of inertia and thermophoresis on particle deposition onto a wavy surface has been studied in [11].

In this study, the particle deposition from a stagnation flow onto an axisymmetric wavy disk under the coupling

* Corresponding author.
E-mail address: chiehli@mail.ncku.edu.tw (C.-L. Chen).

0017-9310/$ - see front matter © 2007 Elsevier Ltd. All rights reserved.
doi:10.1016/j.ijheatmasstransfer.2007.09.035

Nomenclature

D	diffusion constant
E	electric field strength (V/cm)
f	dimensionless stream function
I	dimensionless temperature $\frac{T_w - T_\infty}{T_\infty}$
K_f	thermal conductivity
L	wave length
N	particle concentration
Sc	Schmidt number
St_x	local Stanton number
St_m	mean Stanton number
T	temperature
u	r velocity component
V_d	local particle deposition velocity
V_{dm}	mean particle deposition velocity
w	z velocity component
d_p	particle diameter (μm)

Greek symbols

α	thermal diffusivity
v	kinematic viscosity
θ	dimensionless temperature
ξ, η	coordinate

Superscripts

$\bar{}$	dimensional quantity
$'$	differential to r

Subscripts

i, j	grid position
w	surface conditions
∞	conditions far away from the surface

effect of Brownian diffusion, convection, sedimentation, thermophoresis and electrophoresis in a clean room is studied. The transformed governing equations obtained by coordinate transformation are solved by the spline alternating-direction implicit method. The result reveals that electrophoresis will increase the particle deposition effect.

2. Governing equations

Fig. 1 shows the physical model and coordinate diagram of particle deposition process, where the incompressible Newtonian fluid passes through an axisymmetric wavy disk under a uniform electric field E. The fluid contains particle concentration N_∞ with uniform temperature and uniform velocity. The wavy surface is described by $\overline{S}(\bar{r}) = \bar{a}\sin^2(\pi\bar{r}/L)$. The governing equation can be written as

$$\frac{\partial \bar{u}}{\partial \bar{r}} + \frac{\bar{u}}{\bar{r}} + \frac{\partial \bar{w}}{\partial \bar{z}} = 0 \tag{1}$$

$$\bar{u}\frac{\partial \bar{u}}{\partial \bar{r}} + \bar{w}\frac{\partial \bar{u}}{\partial \bar{z}} = \frac{-1}{\rho}\frac{\partial \bar{p}}{\partial \bar{r}} + v\left(\nabla^2 \bar{u} - \frac{\bar{u}}{\bar{r}^2}\right) \tag{2}$$

$$\bar{u}\frac{\partial \bar{w}}{\partial \bar{r}} + \bar{w}\frac{\partial \bar{w}}{\partial \bar{z}} = \frac{-1}{\rho}\frac{\partial \bar{p}}{\partial \bar{z}} + v\nabla^2 \bar{w} \tag{3}$$

$$\bar{u}\frac{\partial T}{\partial \bar{r}} + \bar{w}\frac{\partial T}{\partial \bar{z}} = \alpha\nabla^2 T \tag{4}$$

$$\bar{u}\frac{\partial \overline{N}}{\partial \bar{r}} + \bar{w}\frac{\partial \overline{N}}{\partial \bar{z}} + \frac{\partial(\bar{u}_t \overline{N})}{\partial \bar{r}} + \frac{\partial((\bar{w}_t + \bar{w}_g + \bar{w}_e)\overline{N})}{\partial \bar{z}} = D\nabla^2 \overline{N} \tag{5}$$

where $\nabla^2 = \frac{\partial^2}{\partial \bar{r}^2} + \frac{1}{\bar{r}}\frac{\partial}{\partial \bar{r}} + \frac{\partial^2}{\partial \bar{z}^2}$. $\bar{w}_g$ and $\bar{w}_e$ are sedimentation and electrophoretic velocity. $\bar{w}_g$ and $\bar{w}_e$ cab be obtained by equating the stokes drag to the gravitational force and coulomb force [4] as

$$\bar{w}_g = -\frac{\rho_p d_p^2 C}{18\mu_g} g \tag{6}$$

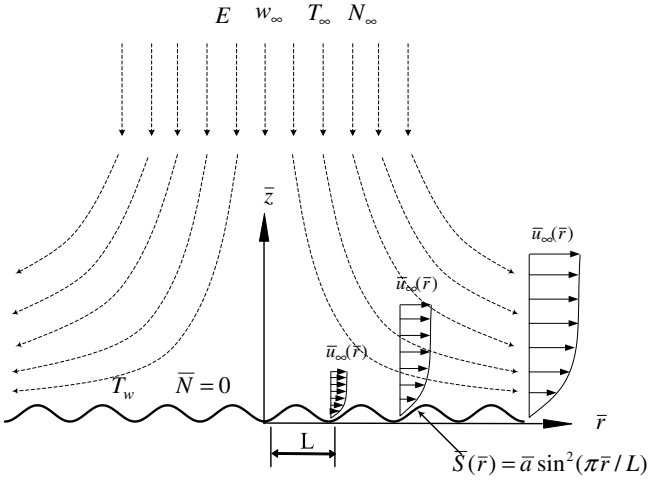

Fig. 1. Physical model.

$$\bar{w}_e = -\frac{n_e e C}{3\pi d_p \mu_g}\vec{E} \tag{7}$$

The thermophoretic velocity recommended by [1] is

$$\bar{u}_t = -k_t v\frac{\nabla T}{T} \tag{8}$$

$$\bar{w}_t = -k_t v\frac{\nabla T}{T} \tag{9}$$

where μ_g, C, and ρ_p are the air viscosity, the Stokes–Cunningham correction factor, and the density of aerosol particle, respectively. d_p and g are particle diameter and the gravitational constant. E, e, and n_e are electric field strength, electron charge, and number of elementary charges. v is thermophoretic diffusivity and k_t is thermophoretic coefficient defined by

$$k_t = \frac{2C_s(\lambda_g/\lambda_p + C_t Kn)C}{(1+3C_m Kn)(1+2\lambda_g/\lambda_p + 2C_t Kn)} \tag{10}$$

with the Knudsen number $Kn = \frac{2\lambda}{d_p}$, which is the ratio of mean free path of aerosol particle to particle diameter. λ_g is the thermal conductivity of air and λ_p is the thermal conductivity of aerosol particles. Constants $C_s = 1.147$, $C_t = 2.20$, $C_m = 1.146$ are determined by experimental data [12]. C is the experimental constant suggested in [13] as

$$C = 1 + Kn(1.2 + 0.41e^{-0.88/Kn}) \tag{11}$$

The boundary conditions are

$$\bar{z} = \overline{S}(\bar{r}) : T = T_w, \quad \bar{u} = \bar{w} = \overline{N} = 0 \tag{12}$$

$$\bar{z} \to \infty : T = T_\infty, \quad \overline{N} = N_\infty, \quad \bar{u} = \bar{u}_\infty(\bar{r}), \quad \bar{p} = \bar{p}_\infty(\bar{r}) \tag{13}$$

where $\bar{u}_\infty$ is the $\bar{r}$ component of the inviscid velocity at outer velocity boundary layer.

Define velocity component with stream function $\bar{\psi}(\bar{r}, \bar{z})$ as

$$\bar{u} = \frac{\partial \bar{\psi}}{\partial \bar{z}}, \quad \bar{w} = -\frac{\partial \bar{\psi}}{\partial \bar{r}} - \frac{\bar{\psi}}{\bar{r}} \tag{14}$$

Then, define the coordinate transformation as

$$\xi = \frac{\bar{r}}{L}, \quad \eta = (\bar{z} - \overline{S})\sqrt{\bar{u}_\infty / \nu \bar{r}} \tag{15}$$

and the dimensionless variable as

$$\begin{aligned} f &= \frac{\bar{\psi}}{\sqrt{\nu \bar{r} \bar{u}_\infty}}, \quad \theta = \frac{T - T_\infty}{T_w - T_\infty}, \quad p = \frac{\bar{p}}{\rho U_0^2}, \quad u_\infty \\ &= \frac{\bar{u}_\infty}{U_0}, \quad Re = \frac{U_0 L}{\nu}, \quad Pr = \frac{\nu}{\alpha}, \quad N = \frac{\overline{N}}{N_\infty}, \quad w_g \\ &= \bar{w}_g / \sqrt{U_0 \nu / L}, \quad Sc = \frac{\mu}{\rho D}, \quad I = -\frac{T_w - T_\infty}{T_\infty} \\ &= -\frac{\Delta T}{T_\infty}, \quad U_0 = a_f L \end{aligned} \tag{16}$$

where $U_0 = a_f L$ is the reference velocity. a_f is the flow strength of stagnation flow as

$$a_f = \frac{2 w_\infty}{\pi R} \tag{17}$$

which can be estimated using the matching flow near the stagnation point with the viscous flow model [5] and R is the radius of the disk.

Using the coordinate transformation, the irregular wavy surface is transformed into a flat surface. The transformed equations are

$$\begin{aligned} &\sigma f''' + \left(\frac{3}{2} f + \xi\left(\frac{f}{2}\frac{u'_\infty}{u_\infty} + f_\xi\right)\right) f'' - \xi \frac{p_\xi}{u_\infty^2} \\ &\quad + \left(S' \sqrt{Re \xi / u_\infty^3} + \frac{\eta}{2u_\infty^2}\left(1 - \xi \frac{u'_\infty}{u_\infty}\right)\right) p' \\ &\quad = \xi\left(f'_\xi f' + \frac{u'_\infty}{u_\infty} f'^2\right) + \frac{\prod_1(f)}{Re^{1/2}} + \frac{\prod_2(f)}{Re} \end{aligned} \tag{18}$$

$$\begin{aligned} &\sigma f''' + \left(\frac{3}{2} f + \xi\left(\frac{f}{2}\frac{u'_\infty}{u_\infty} + f_\xi\right)\right) f'' - S'^{-1} \sqrt{Re \xi / u_\infty^3}\, p' \\ &\quad = \xi\left(f'_\xi f' + \left(\frac{S''}{S'} + \frac{u'_\infty}{u_\infty}\right) f'^2\right) + \frac{\prod_3(f)}{Re^{1/2}} + \frac{\prod_4(f)}{Re} \end{aligned} \tag{19}$$

$$\begin{aligned} &\frac{\sigma}{Pr}\theta'' + \frac{1}{2}\left(3 + \xi \frac{u'_\infty}{u_\infty}\right) f\theta' \\ &\quad = \xi(f'\theta_\xi - f_\xi \theta') + \frac{\prod_5(f,\theta)}{Re^{1/2}} + \frac{\prod_6(f,\theta)}{Re} \end{aligned} \tag{20}$$

$$\begin{aligned} &\frac{\sigma}{Sc} N'' + \left(\frac{f}{2}\left(3 + \xi \frac{u'_\infty}{u_\infty}\right) - (w_g + w_e)\left(\frac{\xi}{u_\infty}\right)^{1/2}\right) N' \\ &\quad - \frac{I k_t \sigma}{1 - I\theta}\left(\frac{IN}{1 - I\theta}\theta'^2 + N'\theta' + N\theta''\right) \\ &\quad = \xi(f' N_\xi - f_\xi N') + \frac{\prod_7(f,N)}{Re^{1/2}} + \frac{\prod_8(f,N)}{Re} \end{aligned} \tag{21}$$

where $\sigma = 1 + S'^2$.

Eq. (18) indicates that $\partial p/\partial \eta$ is $O(Re^{-1/2})$. This implies that the $\partial p/\partial \xi$ can be determined by the inviscid flow outside the boundary layer as the following:

$$p_\xi = -(\sigma u_\infty u'_\infty + S' S'' u_\infty^2) \tag{22}$$

For a large Reynolds number, $\partial p/\partial \eta$ in Eqs. (18) and (19) can be eliminated according to boundary layer theory. By order magnitude analysis, $\prod_1 \sim \prod_8$ can also be neglected. Then the boundary layer equations are obtained as

$$\begin{aligned} &\sigma f''' + \frac{1}{2}\left(3 + \xi \frac{u'_\infty}{u_\infty}\right) f f'' - \xi\left(\frac{S' S''}{\sigma} + \frac{u'_\infty}{u_\infty}\right)(f'^2 - 1) \\ &\quad = \xi(f'_\xi f' - f_\xi f'') \end{aligned} \tag{23}$$

$$\frac{\sigma}{Pr}\theta'' + \frac{1}{2}\left(3 + \xi \frac{u'_\infty}{u_\infty}\right) f\theta' = \xi(f'\theta_\xi - f_\xi \theta') \tag{24}$$

$$\begin{aligned} &\frac{\sigma}{Sc} N'' + \left(\frac{f}{2}\left(3 + \xi \frac{u'_\infty}{u_\infty}\right) - (w_g + w_e)\left(\frac{\xi}{u_\infty}\right)^{1/2} - \frac{I k_t \sigma}{1 - I\theta}\theta'\right) N' \\ &\quad - \frac{I k_t \sigma}{1 - I\theta}\left(\frac{I}{1 - I\theta}\theta'^2 + \theta''\right) N = \xi(f' N_\xi - f_\xi N') \end{aligned} \tag{25}$$

The corresponding boundary conditions are

$$\theta = 1, \quad f = N = 0, \quad f' = 0 \quad \text{as} \quad \eta = 0 \tag{26}$$

$$\theta = 0, \quad f' = N = 1 \quad \text{as} \quad \eta \to \infty \tag{27}$$

Before solving these equations, $\bar{u}_\infty$ should be determined first. In this study, we solve the potential flow by coordinate transformation and SOR method. Stream function and coordinate transformation can be written as below

$$\frac{\partial^2 \bar{\psi}}{\partial \bar{r}^2} + \frac{1}{\bar{r}}\frac{\partial \bar{\psi}}{\partial r} - \frac{\bar{\psi}}{\bar{r}^2} + \frac{\partial^2 \bar{\psi}}{\partial \bar{z}^2} = 0 \tag{28}$$

$$r = \bar{r}/L, \quad z = (\bar{z} - \overline{S})/L \tag{29}$$

Substituting (29) into (28) yields

$$\begin{aligned} &\frac{\partial^2 \psi}{\partial r^2} + \frac{1}{r}\frac{\partial \psi}{\partial r} - \left(\frac{S'}{r} + S''\right)\frac{\partial \psi}{\partial z} - 2S'\frac{\partial^2 \psi}{\partial r \partial z} - \frac{\psi}{r^2} + \sigma \frac{\partial^2 \psi}{\partial z^2} = 0 \\ &u_\infty = \left.\frac{\partial \psi}{\partial z}\right|_{z=0} \end{aligned} \tag{30}$$

The local Stanton number is defined as

$$St = \frac{-V_d}{\bar{u}_\infty} = \frac{-J(\bar{r})}{\bar{u}_\infty N_\infty} \tag{31}$$

where J is particle flux to the wavy surface written as

$$J(\bar{r}) = \left(-D\frac{\partial \overline{N}}{\partial n} + (\bar{w} + \bar{w}_t + \bar{w}_g + \bar{w}_e)\overline{N}\right)_{\bar{z}=\overline{S}(\bar{r})} \tag{32}$$

and $\frac{\partial \overline{N}}{\partial n}$ is the particle gradient perpendicular to the wall. $\bar{w}$, $\bar{w}_t$, $\bar{w}_g$ and $\bar{w}_e$ are fluid velocity, thermophoretic velocity, sedimentation velocity and electrophoretic velocity perpendicular to the wall, respectively. Substituting (32) into (31) with the particle concentration being zero on the wall, it obtains

$$(Re_{\bar{r}})^{1/2} St_{\bar{r}} = \frac{1}{Sc}\sqrt{\sigma\left(\frac{u_\infty}{\xi}\right)}N'|_{z=0} \tag{33}$$

Also, the mean Stanton number is defined as

$$St_m = \frac{-J_m(\bar{r})}{\bar{u}_{\infty,0} N_\infty} \tag{34}$$

$$\text{where} \quad J_m(\bar{r}) = \frac{1}{\pi \bar{r}^2}\int_0^{\bar{r}} 2\pi \bar{r}\sqrt{\sigma} J \mathrm{d}\bar{r} \tag{35}$$

Substitute (35) into (34) and the equation simplifies to

$$(Re_{\bar{r}})^{1/2} St_m = \frac{2}{\xi^2}\int_0^{\xi} \sigma\sqrt{\xi u_\infty} N'|_{z=0}\mathrm{d}\xi \tag{36}$$

Furthermore, local particle deposition velocity and mean particle deposition velocity can be defined as

$$V_d = \frac{\sqrt{v\alpha\sigma u_\infty/\xi}}{Sc} N'|_{\eta=0} \tag{37}$$

$$V_{dm} = \frac{2\sqrt{v\alpha}}{Sc\xi^2}\int_0^{\xi} \sigma\sqrt{\xi u_\infty} N'|_{\eta=0}\mathrm{d}\xi \tag{38}$$

3. Numerical method

Using the spline alternating-direction implicit method and backward differenced, Eqs. (23)–(25) can be expressed in standard form [14,15] as

$$g_{i,j}^{n+1} - G_{i,j} g_{i,j}'^{n+1} - S_{i,j} g_{i,j}''^{n+1} = F_{i,j} \tag{39}$$

where g represents f', θ and N. Hence, Eqs. (23)–(25) yield

$$\begin{aligned}
&\left(\frac{-1}{\Delta\tau} - \xi\left(f_\xi'^{n+1} + \left(\frac{S'S''}{\sigma} + \frac{U'_\infty}{U_\infty}\right)f'^{n+1}\right)\right)f'^{n+1} \\
&\quad + \left(\frac{1}{2}\left(3 + \xi\frac{U'_\infty}{U_\infty}\right)f + \xi f_\xi\right)f''^{n+1} + \sigma f'''^{n+1} \\
&\quad = \frac{-f'^n}{\Delta\tau} - \xi\left(\frac{S'S''}{\sigma} + \frac{U'_\infty}{U_\infty}\right)
\end{aligned} \tag{40}$$

$$\begin{aligned}
&\frac{-1}{\Delta\tau}\theta^{n+1} + \left(\xi f_\xi^n + \frac{f^n}{2}\left(3 + \xi\frac{U'_\infty}{U_\infty}\right)\right)\theta'^{n+1} + \frac{\sigma}{Pr}\theta''^{n+1} \\
&\quad = \frac{-\theta^n}{\Delta\tau} + \xi f'^{n+1}\theta_\xi^{n+1}
\end{aligned} \tag{41}$$

$$\begin{aligned}
&\left(\frac{-1}{\Delta\tau} - \frac{Ik_t\sigma}{1 - I\theta^{n+1}}\left(\frac{I(\theta'^{n+1})^2}{1 - I\theta^{n+1}} + \theta''^n\right)\right)N^{n+1} \\
&\quad + \left(\xi f_\xi^n + \frac{f^n}{2}\left(3 + \xi\frac{U'_\infty}{U_\infty}\right) - \frac{Ik_t\sigma}{1 - I\theta^{n+1}}\theta'^{n+1}\right. \\
&\quad \left. -(w_g + w_e)\sqrt{\frac{\xi}{U_\infty}}\right)N'^{n+1} \\
&\quad + \frac{\sigma}{Sc}N''^{n+1} = \frac{-N^n}{\Delta\tau} + \xi f'^{n+1}N_\xi^{n+1}
\end{aligned} \tag{42}$$

Then, using cubic spline collocation relations, the tridiagonal form of Eqs. (40)–(42) can be expressed as their tridiagonal form

$$A_i g_{i-1}^{n+1} + B_i g_i^{n+1} + C_i g_{i+1}^{n+1} = D_i \tag{43}$$

where g represents second derivatives. Eq. (43) is easily solved by the Thomas algorithm. The numerical procedure is as the following:

1. Obtain $\bar{u}_\infty$ from Eq. (30).
2. Set the boundary conditions and initial values.
3. Solve the steady solution at $z = 0$. It means that f', θ and N satisfy the convergence criteria.
4. Solve the steady solution of next position $z_{i+1} = z_i + \Delta z$ by using the solution of last position. The convergence criteria is

$$\left|\frac{\phi_{i,j}^{k+1} - \phi_{i,j}^k}{\phi_{i,j}^k}\right| \leqslant 10^{-5},$$

   where ϕ represents f', θ and N, and k denotes the number of iterations.
5. Repeat these steps to maximum x.

4. Results and discussion

To confirm the accuracy of the numerical simulation, the resulting local and mean Stanton numbers for different grid sizes are calculated as shown in Table 1. The difference between those results is small and the calculation procedure of non-uniform grids would not be more inextricable than uniform grids for spline alternating-direction implicit method. Hence, a non-uniform grid (600×100) is adopted in this study, where smaller spacing mesh points are used in the neighborhood of the wall. The environmental conditions of particle deposition onto a flat surface are referred to the experiments conducted by Ye et al. [4] with $\rho_p = 1027\ \mathrm{kg\ m^{-3}}$, $T = T_\infty = 300\ \mathrm{K}$, $Pr = 0.72$ and $w_\infty = 30\ \mathrm{cm\ s^{-1}}$. The flat surface considered is a horizontal disk of radius 5 cm. From Eq. (17), the corresponding flow strength a_f is $3.82\ \mathrm{s^{-1}}$.

Figs. 2 and 3 show that the results of flat surface under the effect of thermophoresis and electrophoresis compared with the experiment data [4,7]. The comparison shows good agreement between the experimental data and numerical results obtained by the proposed method, which gives a

Table 1
Solutions obtained by different grid sizes

Grid size	$x = 3$	
	Solutions for $d_p = 1$, $a = 0.01$, $Pr = 0.7$, $E = 10$	
	$(Re_{\bar{r}})^{1/2} St_{\bar{r}}$	$(Re_{\bar{r}})^{1/2} St_m$
900×200	0.004174	0.004182
600×100	0.004177	0.004186
600×50	0.004191	0.00420
300×100	0.004176	0.004186
300×50	0.004190	0.00420

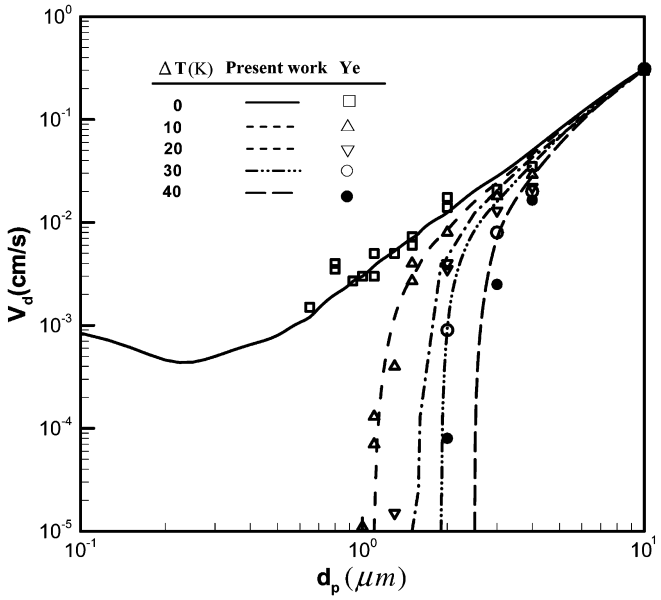

Fig. 2. A comparison of numerical results to the experimental data [4] with different temperature.

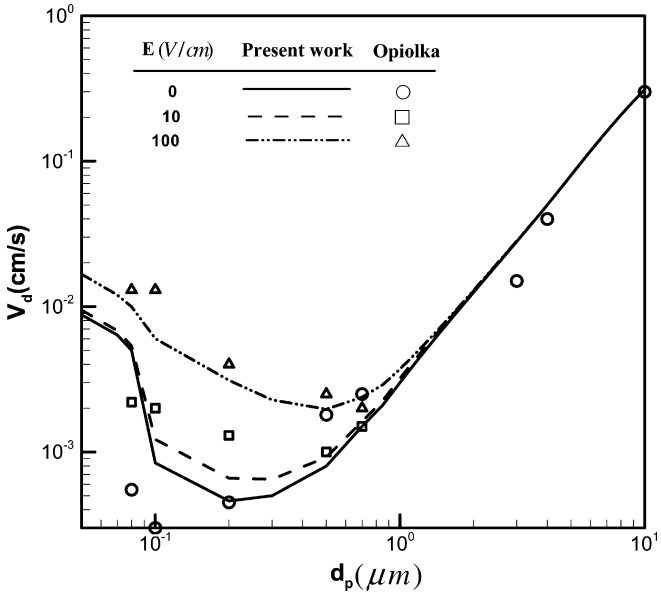

Fig. 3. A comparison of the numerical result to the experimental data [7] with different electric field.

strong support to the proposed approach for particle deposition problem.

In this study, the wavy surface described by $S(\xi) = a\sin^2(\pi\xi)$ is adopted to simulate the particle deposition onto a wavy surface, where a is the amplitude-wavelength (AW) ratio. Fig. 4 is the distribution of local deposition velocity along a wavy surface under different AW ratio and d_p at $I = 0$ and $E = 0$ V/cm. Fig. 5a and b are the distribution schematic diagrams of flow velocity and particle concentration field for $a = 0.02$. Fig. 4 reveals that local deposition velocity for particles of various diameters is constant on a flat plate ($a = 0$), however, local deposition velocity varies with the deposition surface geometry of the wavy plate. Its variation amplitude increases with the increase of the AW ratio and disk radius. Comparing the results of different particle sizes, small particle ($d_p = 0.01$–0.1 μm) is influenced more strongly by the AW ratio. Fig. 5a and b show that velocity and particle concentration increase with the increase of the disk radius. Therefore, convection and Brownian diffusion are dominant deposition mechanisms for small particle. Fig. 5c shows particle concentration with $d_p = 10$ μm is less significantly affected by AW ratio. This means that for large particle, convection and Brownian diffusion are not major factors in the deposition mechanism. Alternatively, sedimentation effect becomes dominant.

Fig. 6 is the distribution of local deposition velocity along wavy surface under different AW ratio and d_p at $I = 0$ and $E = 10$ V/cm. Comparing with Fig. 4, the deposition velocity is not significantly related with particle size. However, electrophoresis promotes more deposition velocity for small particle. Fig. 7 is the distribution of local deposition velocity along wavy surface under different AW ratio and electric field strength at $I = 0.02$ and $d_p = 0.1$ μm. It can be found that electrophoresis effect

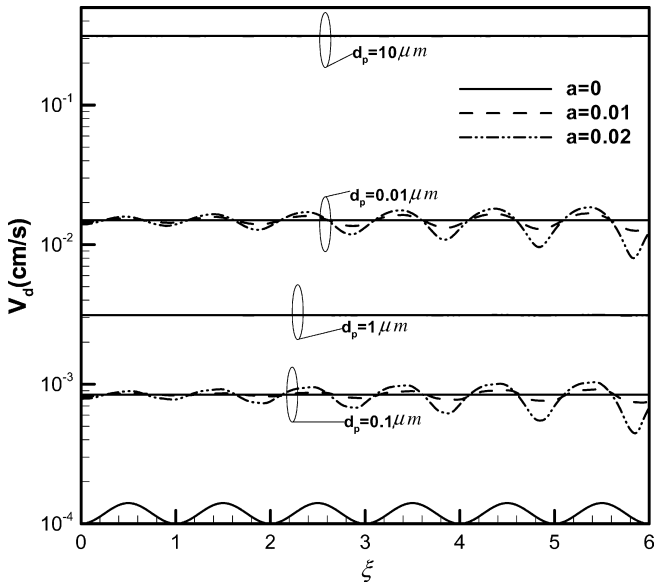

Fig. 4. The distribution of local deposition velocity under different d_p and AW ratio ($I = 0$, $E = 0$).

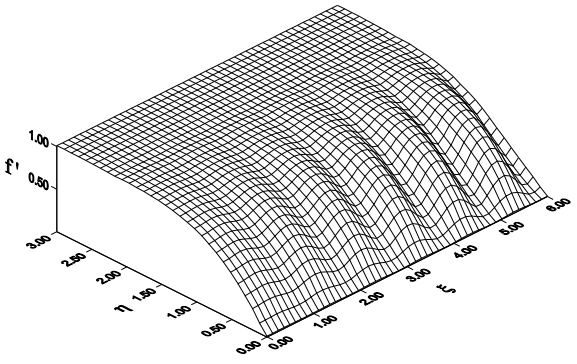

(a) Distribution of velocity field

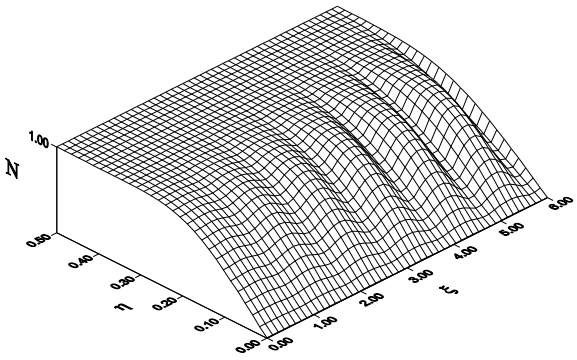

(b) Distribution of particle concentration (d_p=0.01)

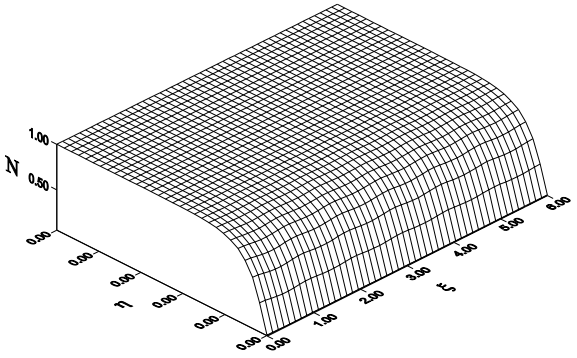

(c) Distribution of particle concentration (d_p=10)

Fig. 5. Distribution of velocity of dimensionless flow field f' and different particle concentration N when AW ratio is 0.02.

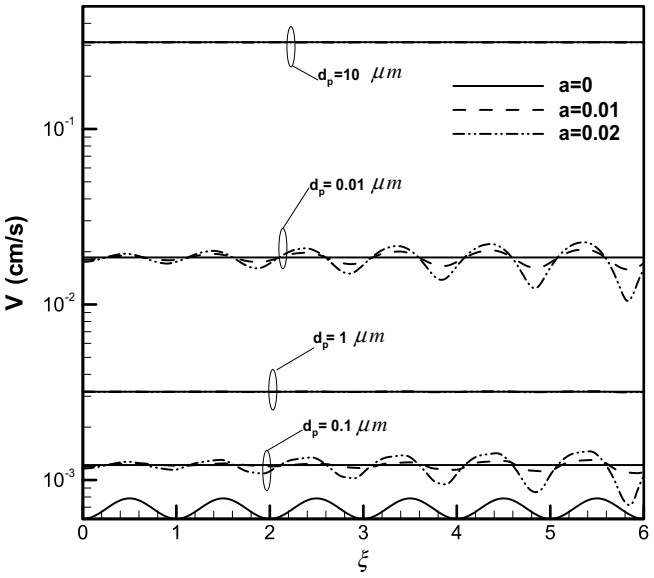

Fig. 6. The distribution of local deposition velocity under different d_p and AW ratio ($I = 0$, $E = 10$).

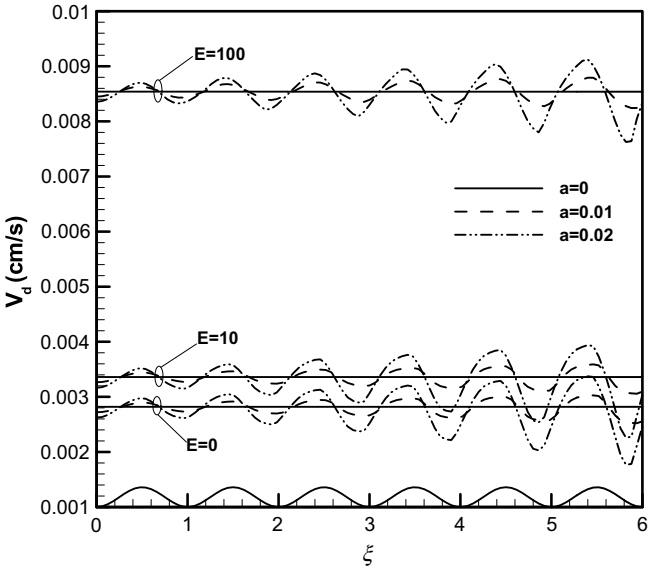

Fig. 7. The distribution of local deposition velocity under different electric field and AW ratio ($I = 0.02$, $d_p = 0.1$).

becomes significant as electric field strength increases. Figs. 6 and 7 reveal that electrophoresis replaces diffusion gradually as a dominate deposition mechanism for small particles, while increasing the electric field strength. For large particles, particle deposition is still dominated by sedimentation effect. In addition, because electric field is constant on the disk, the amplitude of deposition velocity curve does not increase with the increase of electric force. Therefore, the electric field will not alter the original wave pattern.

Fig. 8 is the distribution of local deposition velocity along the wavy surface under different AW ratio and d_p at $I = 0.02$ and $E = 10$ V/cm. Fig. 9 is the distribution of local deposition velocity along wavy surface under different AW ratio and thermophoresis at $E = 100$ and $d_p = 1$ μm. For $I = -0.02$, the periodical distribution of local deposition velocity is related to the geometry of wavy surface with phase shift of 180°. Such phenomenon is caused by the gradual decreasing of Brownian diffusion. In this case, thermophoresis is the major deposition mechanism. The thermophoresis would decrease particle deposition and slow down the deposition velocity for $I = -0.02$. It also shows that the strongest effect of thmophoresis is at the peak of wavy surface, and results a slowest local deposition velocity at the peak.

To investigate the effect of wavy surface on the overall particle deposition effect, Figs. 10 and 11 show the distribution of mean deposition velocity along wavy surface under

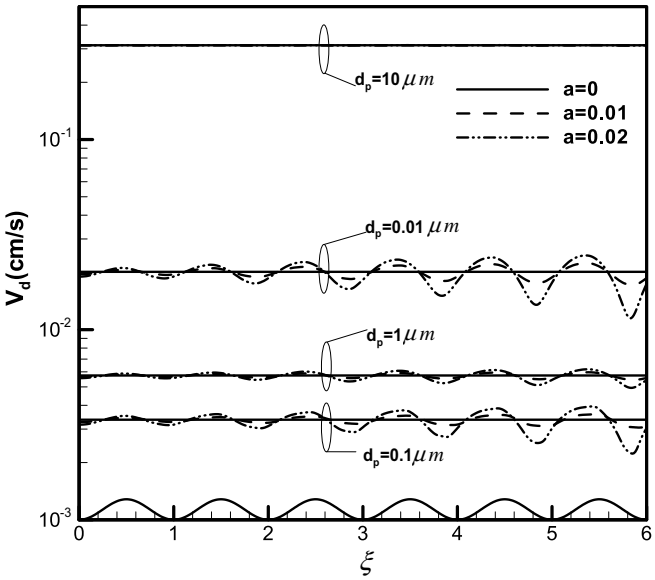

Fig. 8. The distribution of local deposition velocity under different d_p and AW ratio ($I = 0.02$, $E = 10$).

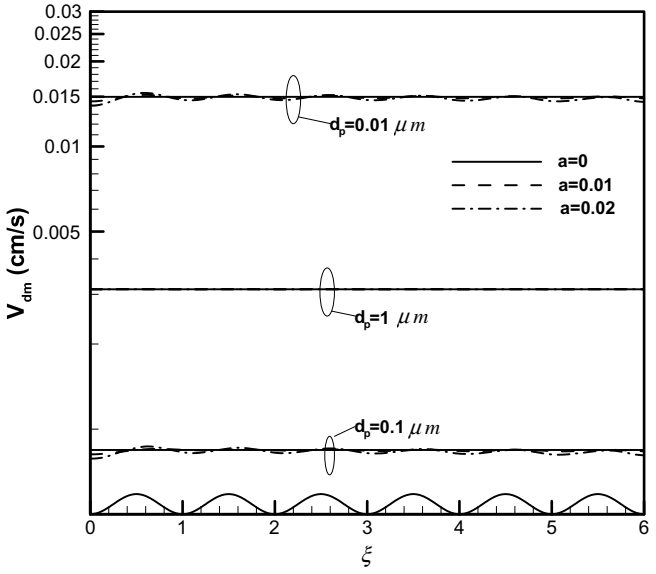

Fig. 10. The distribution of mean deposition velocity under different d_p and AW ratio ($I = 0$, $E = 0$).

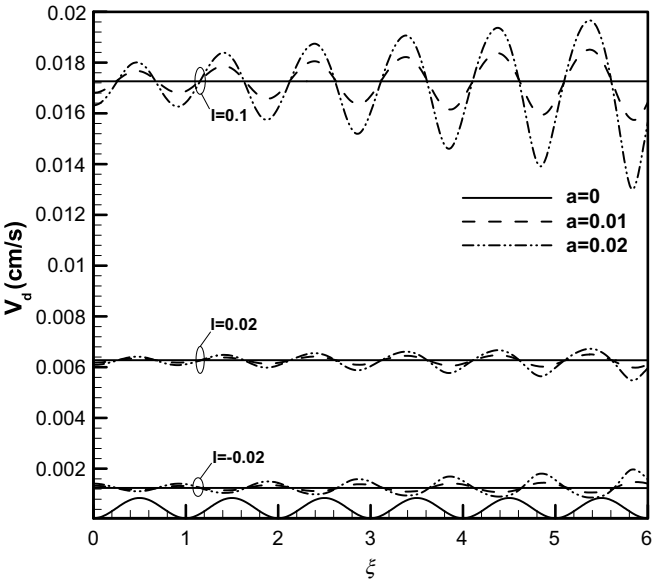

Fig. 9. The distribution of local deposition velocity under different thermophoresis and AW ratio ($E = 100$, $d_p = 1$).

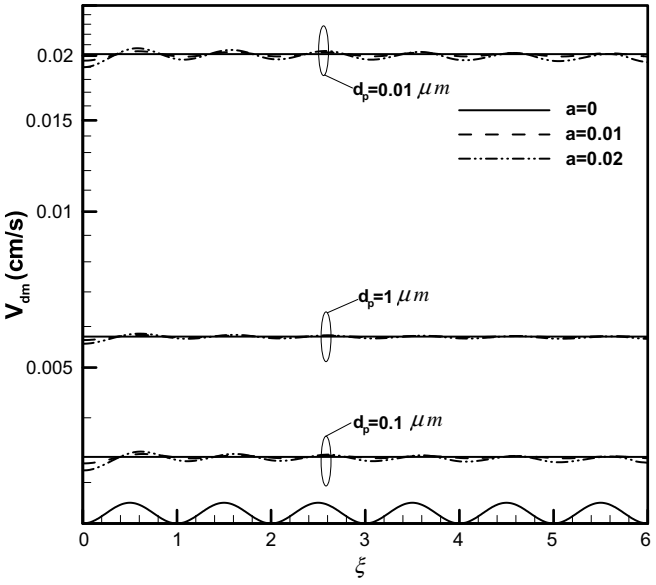

Fig. 11. The distribution of mean deposition velocity under different d_p and AW ratio ($I = 0.02$, $E = 10$).

different electrophoresis and thermophoresis. As mean deposition velocity being the average value of local deposition velocity along the wavy surface, it is found that the variation of mean deposition velocity in the center of the disk is large. Fig. 10 shows that mean deposition velocity of wavy plate is similar to flat plate for large particle ($d_p = 1$ μm). From Fig. 11, under the effect of thermophoresis and electrophoresis, the amplitude of distribution of mean deposition velocity increases as particle size increases. However, the resulting deposition velocity to a wavy surface is similar to that of flat surface with the increase of radius. This is because the influence of sedimentation becomes more significant than thermophoresis and electrophoresis. For small particle, diffusion and thermophoresis are the major deposition mechanisms. The mean deposition velocity of wavy disk would be slightly less than that of flat disk and no significant change on the amplitude with the increase of radius.

5. Conclusions

The paper studied numerically aerosol particle deposition from an axisymmetric stagnation flow onto a wary disc. Thermophoresis, electrophoresis, sedimentation and several factors are taken into consideration. The simulation

results of particle deposition onto a flat plate match well with several earlier experimental works. The same method is then extended to analyze particle deposition onto a wavy disc. Numerical results show that, if the effects of thermophoresis and electrophoresis are left aside, local deposition velocity has a periodic pattern similar to the wavy surface of the disc. Obviously, it is under the influence of the geometric characteristics of the disc. When electrophoretic effect is included, local deposition velocity increases as the strength of electric field increases. Nevertheless, the amplitude of deposition velocity curve still remains unchanged because the AW ratio of wavy disc has no effect on electric field. On the other hand, because the temperature of wavy disc varies with the AW ratio and radius, the temperature gradient near the wavy surface is altered such that thermophoresis become stronger as the radius increases. Therefore, local deposition velocity as well as the amplitude of deposition curve increases as the radius increases due to stronger thermophoretic effect. Though a wavy disc has a larger deposition surface and strong thermophoretic effect that increase particle deposition at the peak of wavy surface, the local deposition velocity in the concave region of wavy disc is relatively slower than that of flat plat. When it comes to comparing a wavy disc with a flat plate with the same projection area, previous factors makes the net effect of overall particle deposition onto a wavy disc less than onto a flat plat. The results also show that while sedimentation effect dominates the particle deposition mechanism when particle size are large, thermophoresis and electrophoresis play more significant roles as particle size reduces. The present work provides a better understanding of the effects of thermophoresis and electrophoresis on particle deposition onto a wavy surface.

Acknowledgement

The work was partly supported by the National Science Council, Taiwan, under the grant No. NSC94-2212-E006-062.

References

[1] L. Talbot, R.K. Cheng, R.W. Scheffer, D.P. Wills, Thermophoresis of particle in a heated boundary layer, J. Fluid Mech. 101 (1980) 737–758.
[2] S.L. Goren, Thermophoresis of aerosol particles in the laminar boundary layer on a flat surface, J. Colliod Interface Sci. 61 (1977) 77–85.
[3] G.M. Homsy, F.T. Geyling, K.L. Walker, Blausius series for thermophoresis deposition of small particles, J. Colliod Interface Sci. 83 (1981) 495–501.
[4] Y. Ye, D.Y.H. Pui, B.Y.H. Liu, S. Opiolka, S. Blumhorst, H. Fissan, Thermophoretic effect of particle deposition on a free standing semiconductor wafer in a clean room, J. Aerosol Sci. 22 (1991) 63–72.
[5] D.W. Cooper, M.N. Perers, R.J. Miller, Predicted deposition of submicrometer particles due to diffusion and electrostatics in viscous axisymmetric stagnation-point flow, J. Aerosol Sci. Technol. 11 (1989) 133–143.
[6] T.W. Peterson, F. Stratmann, H. Fissan, Particle deposition on wafers: a comparison between two modeling approaches, J. Aerosol Sci. 20 (1989) 683–693.
[7] S. Opiolka, F. Schmidt, H. Fissan, Combined effects of electrophoresis and thermophoresis on particle deposition onto flat surfaces, J. Aerosol Sci. 25 (1994) 665–671.
[8] R. Tsai, Y.P. Chang, T.Y. Lin, Combined effects of thermophoresis and electrophoresis on particle deposition onto a wafer, J. Aerosol Sci. 29 (1998) 811–825.
[9] C.C. Wang, C.K. Chen, Transient analysis of forced convection along a wavy surface in micropolar fluids, AIAA J. Thermophys. Heat Transfer 14 (2000) 340–347.
[10] C.C. Wang, C.K. Chen, Transient force and free convection along a vertical wavy surface in micropolar fluids, Int. J. Heat Mass Transfer 44 (2001) 3241–3251.
[11] C.C. Wang, Effect of thermophoresis on particle deposition rate from a natural convection flow onto a vertical wavy plate, Int. Commun. Heat Mass Transfer 32 (2005) 1337–1349.
[12] C. Shen, Thermophoretic deposition of particles onto cold surface of bodies in two dimensional and axi-symmetric flows, J. Colloid Interface Sci. 127 (1989) 104–115.
[13] G.K. Batchelor, C. Shen, Thermophoretic deposition in gas flow over cold surface, J. Colloid Interface Sci. 107 (1985) 21–37.
[14] P. Wang, R. Kahawita, A two-dimensional numerical model of estuarine circulation using cubic spline, Can. J. Civil Eng. 10 (1983) 116–124.
[15] P. Wang, R. Kahawita, Numerical integration of partial differential equations using cubic splines, Int. J. Comput. Math. 13 (1983) 271–286.